RSC Advances

PAPER

View Article Online
View Journal | View Issue

Cite this: *RSC Adv.*, 2025, **15**, 40846

Research on developing SERS substrates based on a ZnO porous membrane decorated with silver nanoparticles aimed at detecting low concentrations of Rhodamine B

Thuy Ngoc Thuy Nguyen,[a] Nhat Tam Ha Nguyen,[bc] Minh Khoi Tran,[bc] Hoai Nhan Luong,[bc] Le Thai Duy,[bc] Hien D. Tong,[d] Thanh Truc Pham[a] and Vinh Quang Dang *[bc]

Recently, Ag-decorated ZnO has been explored for detecting the residual organic toxins through surface-enhanced Raman scattering (SERS), based on the local surface plasmonic resonance (LSPR) effect. In this study, we presented the composite of Ag/ZnO nanoparticles with a porous structure, supported by polystyrene (PS), for fabricating SERS substrates to detect Rhodamine B (RhB) at low concentration. In this structure, Ag nanoparticles (NPs) enhance the Raman signals *via* the electromagnetic mechanism (EM), while ZnO contributes to signal enhancement through the chemical mechanism (CM). PS microspheres improve the adhesion of Ag/ZnO on substrates and enable the formation of a porous structure in the membrane. At an excitation wavelength of 532 nm, the SERS intensity of RhB at 1645 cm^{-1} exhibits a linear relationship with RhB concentration. The limit of detection (LOD) and enhancement factor (EF) for the porous Ag/ZnO structure are calculated to be 7.9×10^{-6} ppm and 3.08×10^{6}, respectively. The innovative porous architecture is advantageous for Raman signal generation and therefore well-suited for detecting residual organic toxins in agricultural products.

Received 20th August 2025
Accepted 15th October 2025

DOI: 10.1039/d5ra06188a

rsc.li/rsc-advances

1. Introduction

Health problems related to food are becoming more of a concern in modern society. One of the biggest issues is food additives, which are substances added to food to preserve or improve its flavor and appearance. There are a huge number of food additives consumed daily, including artificial sweeteners, preservatives, food coloring, *etc.* Unfortunately, many additives have been linked to various health problems, including allergies, digestive issues, and even more serious conditions such as cancer. Among excessively used food additives, synthetic dyes are considered a major threat. One of the most common is Rhodamine B (RhB), which is an industrial azo dye with high water solubility. It has been widely used for fluorescent labeling and food coloring due to its durability, low cost, and stability.[1,2] Some fraudsters often counterfeit corn dye using industrial dye RhB to create fake chili powder or to enhance the natural color of chili powder.[3] However, RhB has potential toxic effects and is an allergen affecting the human respiratory system, skin, and brain.[4,5] In 2024, P. S. Priya *et al.* shown that RhB exposure at a concentration of 1.5 mg L^{-1} could lead to significant impairments in fecundity parameters, particularly affecting females.[6] Therefore, it is necessary to detect RhB as well as residue organic toxic materials remaining in foods to protect human health.

Until now, several analytical methods have been developed for the determination of RhB such as HPLC, HPLC-MS, *etc.* M. Arabi *et al.* used hydrophilic molecularly imprinted nanospheres (MINs), which were subsequently utilized as a dispersant sorbent in matrix solid phase dispersion (MSPD) for the extraction of RhB, followed by HPLC analysis, achieving a limit of detection (LOD) of 0.14 μg kg^{-1}.[7] Also, J. Wu *et al.* achieved a LOD of 0.004 μg mL^{-1} when detecting RhB by the HPLC method.[8] In another publication, RhB was successfully detected in candies by a high-throughput liquid chromatography-tandem mass spectrometry (LC-MS/MS) method with an LOD of 0.09 μg kg^{-1}.[9] Although these analysis methods are reliable and highly accurate for detecting RhB, they require complex pretreatment and costly equipment, making them unsuitable for on-site analysis.[3] Nowadays, surface-enhanced Raman scattering (SERS) is a powerful and promising spectroscopic technique for detecting molecules at ultralow concentrations,

[a]*Faculty of Applied Sciences, HCMC University of Technology and Education, 1 Vo Van Ngan Street, Thu Duc Ward, Ho Chi Minh City 70000, Vietnam*

[b]*Faculty of Materials Science and Technology, University of Science, 227 Nguyen Van Cu Street, Cho Quan Ward, Ho Chi Minh City 70000, Vietnam. E-mail: vinhquangntmk@gmail.com*

[c]*Vietnam National University, Dong Hoa Ward, Ho Chi Minh City 70000, Vietnam*

[d]*Faculty of Engineering, Vietnamese-German University (VGU), Ring Road 4, Quarter 4, Thoi Hoa Ward, Ho Chi Minh City 70000, Vietnam*

fingerprint specificity, and nondestructive sample analysis.[10] As a result, SERS has been widely applied in various analytical fields, including chemical analysis,[2,3] biological analysis,[11] medical diagnostics,[12] environmental monitoring,[13] and food safety.[14] Currently, two main mechanisms that contribute to enhanced SERS signals are EM and CM. Among them, EM plays a dominant role through the LSPR of noble metal nanoparticles. When the plasmonic resonance happens, the electromagnetic field around the metal nanoparticles increases much more rapidly; as a result, it effectively enhances the Raman scattering. Besides, CM is to rely on the interaction between active materials and target molecules leading to the electron transfer. The CM mechanism is less common than the EM mechanism; therefore, very few publications on CM have been presented. To successfully fabricate high-performance SERS substrates, both the structure and active materials need to be developed. Regarding to structural development, S. Yang *et al.* fabricated hybrid CdS/Au flower-like nanomaterials to detect crystal violet, Rhodamine B and malachite green with LODs of 6.30×10^{-9} 8.40×10^{-9}, and 8.60×10^{-8} M, respectively;[15] Linxing Chen *et al.* developed a SERS-active Au@Ag core–shell nanorod (Au@AgNR) tag platform for ultrasensitive bacteria detection and antibiotic-susceptibility testing (AST) and successfully applied to detect *E. coli* with limit of detection as low as 102 330 CFU mL^{-1}.[16] By using nanosilver-embedded silicon nanowires, V.-T. Vo *et al.* had the ability to detect picomolar with an LOD of 10^{-13} M.[17] Besides, developing active materials also plays an important role in reaching high-performance SERS substrates. Using the paper substrate deposited with silver nanoparticles by brush, Rhodamine 6G (R6G) and trace malachite green (MG) were successfully detected with the LOD of 1 nM and 10 nM, respectively.[18] X. Qiu *et al.* used β-cyclodextrin functionalized silver nanoparticles to detect norfloxacin (NFX) in milk with an LOD of 5.327 nmol L^{-1};[19] L. Yang *et al.* used the halide-modified Au nanoparticles to detect bisphenol A residues in milk with an LOD of $4.3.10^{-9}$ mol L^{-1};[20] L. He *et al.* used the hierarchical Cu nanoparticles/rGO (CuNPs/rGO) composites to detect R6G with an LOD of 10^{-8} mol L^{-1}.[21]

Currently, ZnO and Ag are widely used as active materials for SERS applications due to abundant reserves, various morphologies, and diverse synthesis techniques. In 2016, S. Cui *et al.* successfully developed three-dimensional (3D) ZnO/Ag nanowire array (NWA) substrates to detect malachite green (MG) with an LOD of 10^{-12} M.[22] In addition, Taotao Dong *et al.* (2024) fabricated hierarchically porous coralloid ZnO@Ag (C-ZnO@Ag) microspheres to detect MG content in water with an ultralow concentration of 10^{-9} M.[23] However, to fabricate high-performance SERS based on ZnO/Ag, it is necessary to enhance the adhesion between the active materials and the substrates to improve the density distribution. Moreover, the porous structures enable the prolongation of the photon interaction time and boost the photon scattering.

Herein, the porous Ag/ZnO membrane was successfully developed on a silicon substrate, achieving good adhesion and uniformity through polystyrene (PS) nanoparticle coating and thermal treatment. These PS nanoparticles played a crucial role in both improving the uniform density distribution and enabling a porous structure through thermal treatment. The porous structures enhance light scattering *via* prolonging the interaction time between the excitation light source and target molecules. The results demonstrated a high-performance detection limit (LOD) for Rhodamine B at a low concentration of 7.9×10^{-6} ppm. The porous structure gives the new approach to overcome the limitations of Ag/ZnO materials on flat Si substrates.

2. Experimental section

2.1. Chemical materials

The chemicals were used in these experiments, including zinc(II) oxide nanoparticles 40 wt% dispersion in ethanol (ZnO NPs, 99%, Sigma-Aldrich, USA), silver nitrate ($AgNO_3$, 99%, Sigma-Aldrich, USA), hydrogen peroxide (H_2O_2, 30%, Sigma-Aldrich), potassium hydroxide (KOH, 85%, Ghtech, China), D-glucose ($C_6H_{12}O_6$, Ghtech, China), sulfuric acid (H_2SO_4, 95–98%, Xilong Scientific, China), ammonia solution (NH_3, Ghtech, China), and polystyrene nanospheres 10 wt% dispersion in distilled water (PNS, Sigma-Aldrich, USA).

2.2. Synthesis of porous Ag/ZnO membrane

The synthesis of the porous Ag/ZnO membrane begins with the stirring of ZnO NPs (diluted to 1.5% in ethanol) and polystyrene nanospheres (10 wt% in DI water) for 10 min. Firstly, the silicon wafer is treated by piranha that generate hydroxy radicals (OH–) that improve the hydrophilicity of the silicone substrate surface (Fig. 1a). Next, the mixture solution was sprayed onto the pre-prepared silicon surface, then the membrane was soft baked at 50 °C for 15 minutes. Before silver nanoparticle (Ag NP) decorating, the sample was annealed at 400 °C for 1 h to form the porous structure. Ag NPs decorated onto the ZnO porous membrane process were presented in Fig. 1b *via* a chemical method following our previous paper.[24,25]

2.3. Characterizations

The surface morphology and elemental composition were examined using a scanning electron microscope-energy dispersive X-ray analyzer (SEM-EDX, Hitachi S-4800). The crystal structures of ZnO NPs with and without Ag NPs were observed by X-ray diffraction (XRD) performed on the D8 Advance-Bruker diffractometer operating at 40 kV, 100 mA with the Cu/K α radiation source ($\lambda = 0.154$ nm). The optical properties of the samples were determined through diffuse reflectance ultraviolet-visible spectroscopy (Jasco V770). Raman spectra were recorded by a Raman spectrometer (Xplora One, HORIBA) with the excitation source at a wavelength of 532 nm, a capacity of 5 mW, a 10× objective lens, and the acquisition time was adjusted to 15 s for each spectrum.

3. Results and discussions

3.1. The characterization of Ag NPs decorated porous ZnO membrane

The optical images of the sample surface (Fig. 2) are used to evaluate the adhesion capability of Ag/ZnO porous membrane

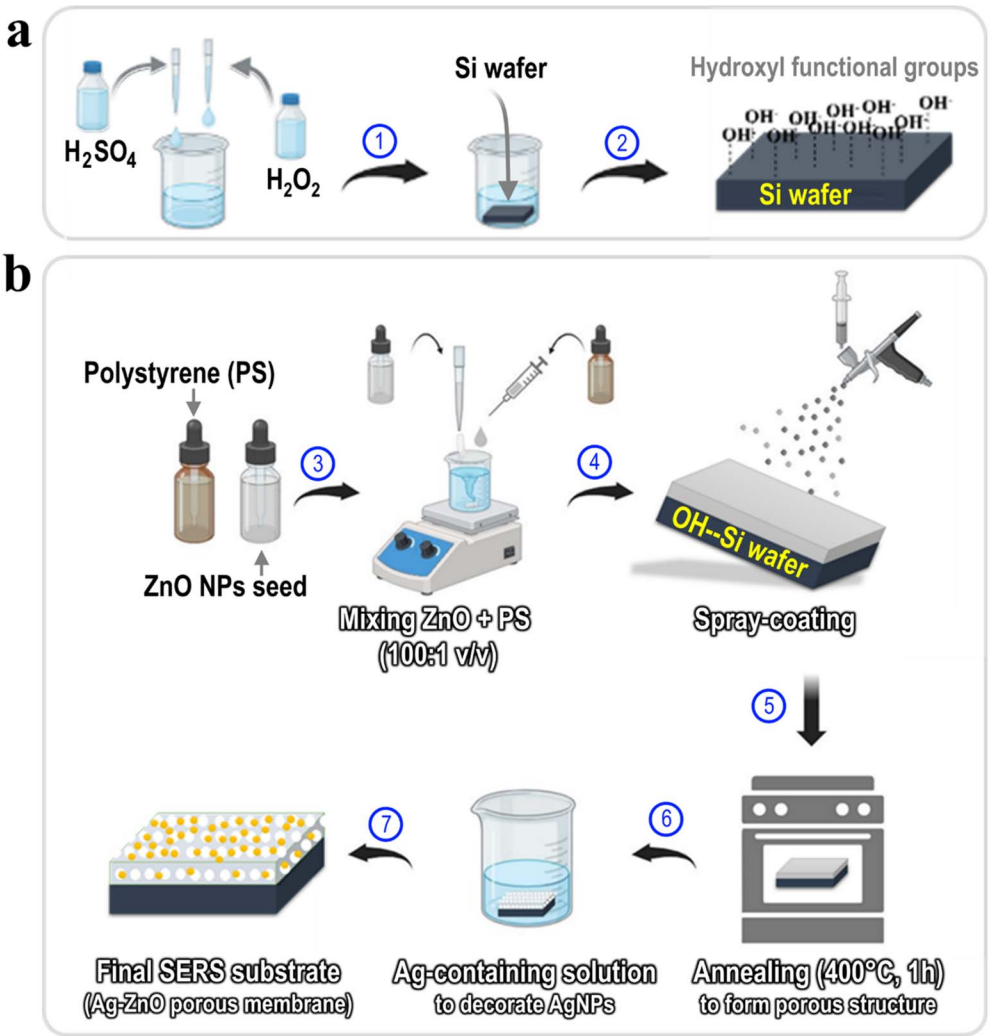

Fig. 1 (a) Piranha treatment silicone substrates. (b) Illustrating synthesis process of Ag/ZnO porous membrane on silicon wafer.

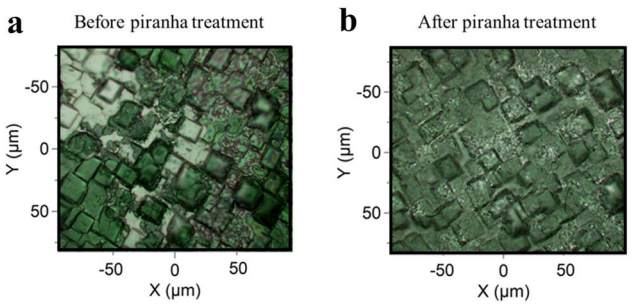

Fig. 2 Surface morphologies of Ag/ZnO porous membranes (a) without and (b) with Si piranha treatment.

on the silicon substrate in case of Si with and without piranha treatment. Indeed, the silicon surface exhibits hydrophobic behavior that prevents the adhesion of Ag/ZnO to the substrate surface (Fig. 2a). With piranha treatment, the hydrophobic surface is transferred to hydrophilic due to the formation of Si–O bonds on the surface. Therefore, the Ag/ZnO film exhibits more uniformity and higher density that one is nontreatment (Fig. 2b).

The morphology of our Ag/ZnO membrane was examined as shown in SEM images in Fig. 3a, SI Fig. S1a and b. The nanoparticles are uniformly distributed in ZnO membrane with the thickness of approximately 4.5 μm (as confirmed in SI Fig. S1a). Besides, the porous structure, observed in the sample's morphology, exhibits a high density of uniformly distributed pores throughout the matrix, with mostly nanopores having diameters below 300 nm, as shown in SI Fig. S1c. The EDX mapping of the Ag/ZnO porous membrane (Fig. 3b) shows the even distribution of Si, Zn, O, and Ag elements within the matrix. Notably, it further confirms that the silver nanoparticles (Ag NPs) exist uniformly in porous membrane. The XRD patterns of ZnO porous membrane with and without Ag NPs decorating are revealed in Fig. 3c. Both samples show the characteristic diffraction peaks of ZnO with hexagonal wurtzite structure at position $2\theta = 31.75°$, 34.43°, 36.23°, 47.54°, 62.87°, and 56.61° which corresponded to (100), (002), (101), (102), (110), and (103) planes (JCPDS No. 36-1451). Additionally, a new

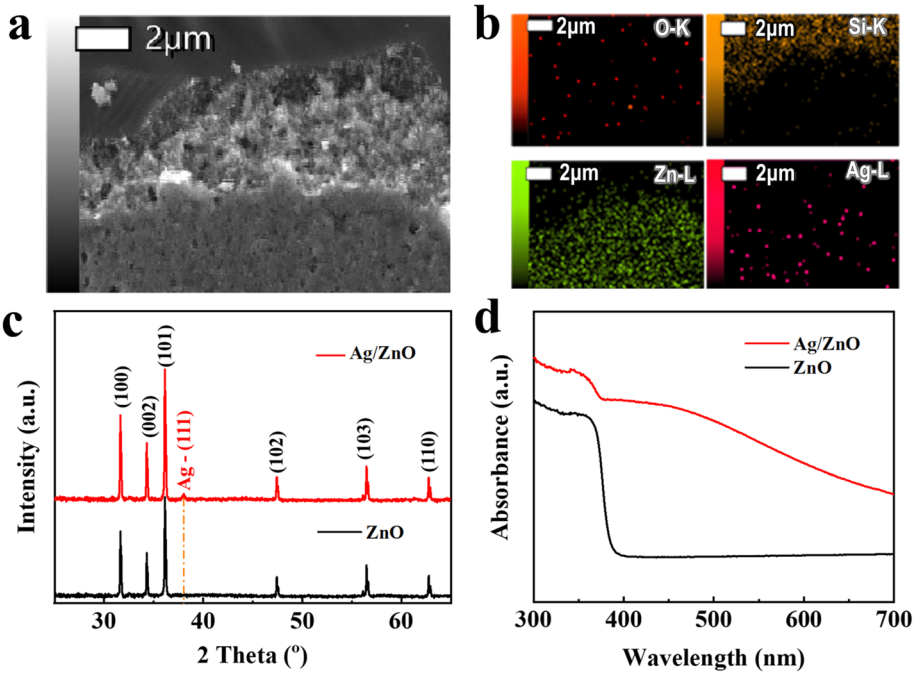

Fig. 3 (a) SEM image and (b) elemental composition of the Ag–ZnO porous membrane and, (c) XRD pattern and (d) diffuse reflectance spectra of the pure ZnO porous membrane (black line) and Ag–ZnO porous membrane (red line).

peak consistently appeared in the sample of Ag/ZnO porous membrane at $2\theta = 38.18°$, corresponding to the crystal plane (111). These characteristic peaks demonstrated the Ag crystal structures (JCPDS 04-0783). In addition, optical properties of both samples are revealed by diffuse reflectance spectra in Fig. 3d. It shows the sharp absorption edge of the ZnO porous membrane in the ultraviolet region with an absorption peak of about 362 nm ($E = 3.42$ eV) due to band-to-band electronic transitions.[26] Interestingly, a wide absorption range from about 400 nm to 600 nm, and the maximum peak is at about 460 nm is observed in Ag/ZnO membrane. It is attributed to the LSPR effect of Ag NPs. The sample Ag/ZnO porous membrane can give a good LSPR effect with the laser excitation wavelength of 532 nm, thereby increasing the electromagnetic (EM) effect and eventually enhancing the SERS effect.

3.2. SERS results for Rhodamine B detection

To evaluate the performance of SERS substrate based on Ag/ZnO porous membrane, the RhB solution of 1 ppm concentration

Table 1 Band assignment of Rhodamine B[27,28]

Solid Raman	SERS	Vibrational description
619 cm^{-1}	620 cm^{-1}	Aromatic bending
1195 cm^{-1}	1197 cm^{-1}	Aromatic C–H bending
1275 cm^{-1}	1279 cm^{-1}	C–C bridge – bands stretching
1356 cm^{-1}	1360 cm^{-1}	Aromatic C–C stretching
1506 cm^{-1}	1509 cm^{-1}	Aromatic C–C stretching
1525 cm^{-1}	1525 cm^{-1}	Aromatic C–C stretching
1595 cm^{-1}	1595 cm^{-1}	C=C stretching
1645 cm^{-1}	1645 cm^{-1}	Aromatic C=C stretch

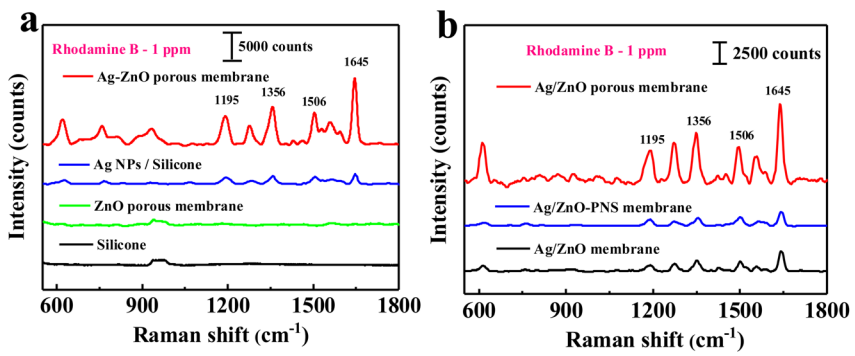

Fig. 4 Raman spectra of Rhodamine B at a concentration of 1 ppm on different substrates (a) bare silicone, ZnO porous membrane/Si, Ag NPs/Si, and Ag/ZnO porous membrane/Si; (b) Ag/ZnO membrane/Si (Ag and ZnO NPs mixed together), Ag/ZnO-PNS membrane/Si (Ag and ZnO NPs mixed with polystyrene nanospheres but without heat treatment) and Ag/ZnO porous membrane/Si.

was dropped onto various substrates including bare silicone, ZnO porous membrane/Si, Ag NPs/Si, and Ag/ZnO porous membrane/Si. Raman spectra of these samples were recorded as shown in Fig. 4a. It is not found any Raman peaks of RhB at both bare silicone and ZnO porous membrane/Si substrates. While for Ag NPs/Si and Ag/ZnO porous membrane/Si samples, the characteristic Raman peaks are clearly observed due to the strong LSPR effect of Ag NPs distributed on these substrates. The Raman signals show the characteristic peaks of RhB at 620, 1197, 1279, 1360, 1509, 1525,1595, and 1645 cm^{-1} corresponding to different bonding and vibrational modes presented in Table 1. The data also shows the peak at 1645 cm^{-1} is the strongest one. In addition, the Raman characteristic peak intensity of RhB adsorbed onto Ag/ZnO porous membrane/Si substrate is significantly enhanced compared to Ag NPs/Si substrate. The data here confirm clearly the role of porous structure of ZnO membrane thereby Ag NPs decorating both onto and into the ZnO porous membrane, as a result, the LSPR effect of Ag NPs was boosted greatly. Therefore, the SERS substrate based on Ag/ZnO porous membrane is able to detect RhB at lower 1 ppm concentration. Fig. 4b provides a specific comparison of Raman spectrum of RhB at 1 ppm concentration on various substrates including Ag/ZnO membrane/Si (Ag and ZnO NPs mixed together), Ag/ZnO-PNS membrane/Si (Ag and ZnO NPs mixed with polystyrene nanospheres but without heat treatment) and Ag/ZnO porous membrane/Si. This highlights the superior enhancement capability of the porous-structured Ag/ZnO membrane. Polystyrene nanospheres (PNS) act as a mean to form porous structure when they are annealed at high temperature 400 °C in 1 h for vaporization, leaving behind a lot of vacancies. PNS also have a role to prevent ZnO nanoparticle aggregation, leading to promote even dispersion of ZnO NPs during thermal processing. The porous structure enhances the light absorption capacity and prolonged the interaction time between the light excitation source and the target molecules. In addition, with a high density of pore and a rough surface, Ag NPs can easily decorate into the porous membrane, improving significantly Raman scattering signal. As evidenced by the peak intensities in Fig. 4b, Ag/ZnO porous membrane exhibits great intensity of RhB characteristic peaks compared to the other samples.

The Raman spectra of RhB at various concentrations from 0 to 1 ppm on SERS substrates based on Ag/ZnO porous membrane are shown in Fig. 5a. The peak intensity decreases as the RhB concentration declines from 1 ppm to 10^{-5} ppm. Moreover, the characteristic peak at 1645 cm^{-1} can be identified even at a concentration of 10^{-5} ppm. Fig. 5b shows a linear relationship between SERS intensities and the logarithm of RhB concentration. The fitting equation is $I = 2551.90606 \times \log [C_{RhB}] + 11546.06648$, and the correlation coefficient R^2 is 0.95045. The limit of detection (LOD) of the SERS substrates can be estimated *via* the equation:[29]

$$\mathrm{LOD} = 3 \times (S_w/b) \quad (3.1)$$

where S_w denotes the standard deviation of the blank sample, and b shows the slope of the calibration curve. The LOD of Ag/ZnO porous membrane SERS substrate in detecting RhB is estimated to be 7.9×10^{-6} ppm *via* eqn (3.1). In addition, this detection limit is quite outstanding compared to some of the

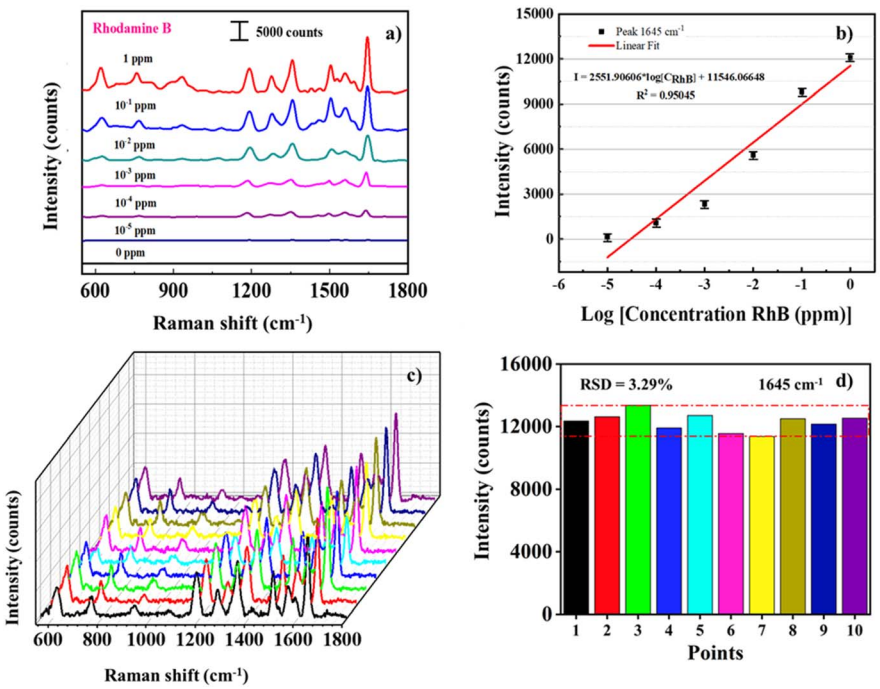

Fig. 5 (a) Raman spectra of Rhodamine B in various concentration from 0 to 1 ppm; (b) the linear relationship of the peak intensity at 1645 cm^{-1} as a function of the Rhodamine B concentration from 10^{-5} to 1 ppm; (c) SERS spectra at 10 positions on the Ag/ZnO porous membrane SERS substrate; (d) Raman intensity of the 1645 cm^{-1} peaks at 10 positions on the Ag/ZnO porous membrane SERS substrate.

Table 2 Comparison of LOD of Ag/ZnO porous membrane SERS with other methods

Techniques	Substrate	Target analyte	Experimental method	LOD (ppm)	Ref.
HPLC	Fe_3O_4@SiO_2@[OMIM]PF_6	Rhodamine B	MSPE/chemical process	8.10^{-2}	31
FL	Fe_3O_4@ILs-β-CDCP	Rhodamine B	MSPE	5.2	32
UV-VIS	Extraction solvent cyclohexylamine	Rhodamine B	Chemical process	1.4×10^{-2}	33
SERS	Au@Au@Ag double shell nanoparticles	Rhodamine B	Chemical process	10^{-4}	34
SERS	Ag@ZnO nanoplates	Methylene blue (MB)	Chemical process	10^{-9}	35
SERS	Ag@ZnO nanoflowers	Thiram	Chemical process	2.4×10^{-6}	36
		Carbendazim		1.8×10^{-4}	
SERS	Ag/ZnO porous membrane	Rhodamine B	Annealing/chemical process	7.9×10^{-6}	This work

previous methods and studies mentioned in Table 2. Besides, the enhancement factor (EF) is an essential indicator for quantifying the performance of the substrate, and the EF for SERS detection is calculated according to the following equation (*via* peak 1645 cm^{-1}):[30]

$$EF = (I_{SERS}/I_{BARE}) \times (C_{BARE}/C_{SERS}) \quad (3.2)$$

where I_{SERS} and I_{BARE} are the intensities of the Raman signals acquired from the SERS substrate and the silicone substrate (I_{SERS} = 0.08 counts, I_{BARE} = 5.18 counts, respectively). C_{SERS}

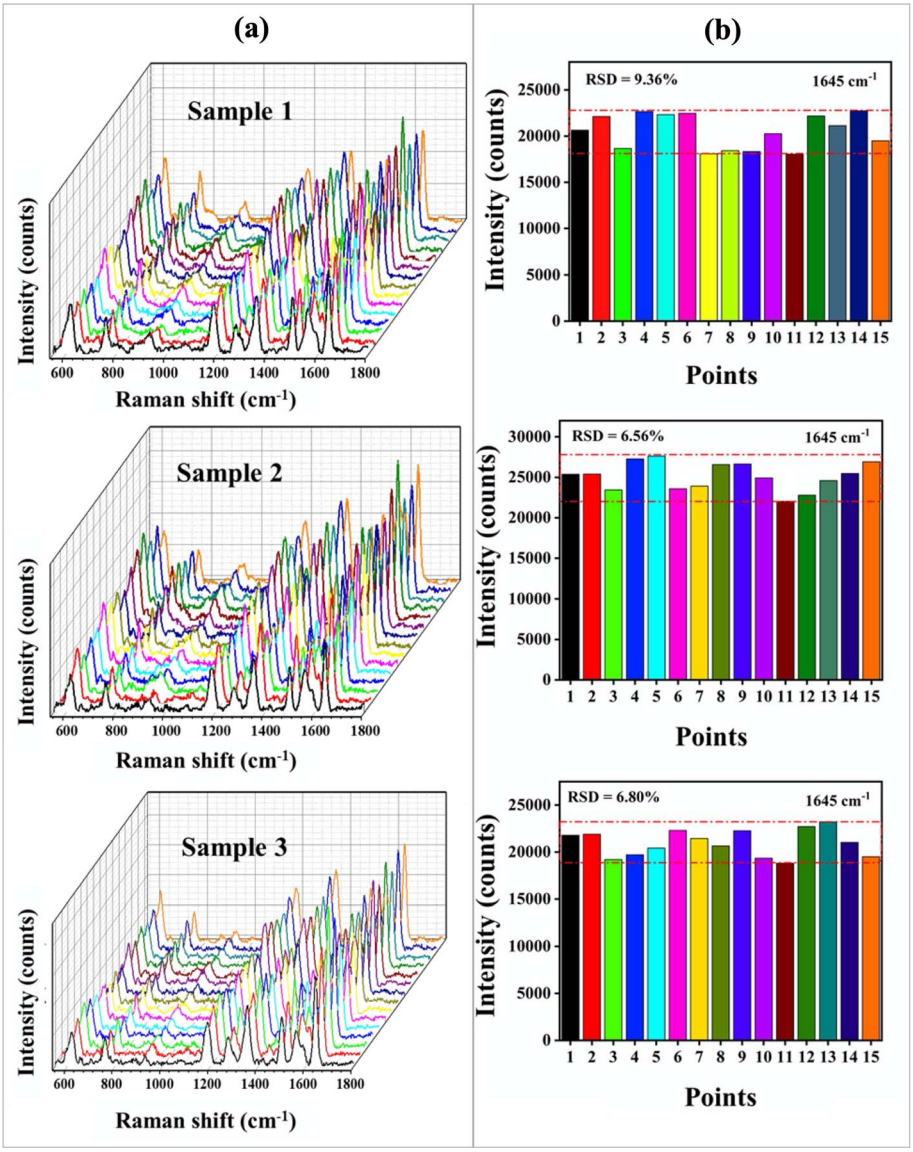

Fig. 6 (a) SERS spectra and (b) SERS intensity of the 1645 cm^{-1} peaks at 15 positions of three different SERS substrates with same experiment conditions.

and C_{BARE} are the concentrations of the RhB solution corresponding to the SERS detection and the normal Raman detection ($C_{SERS} = 10^{-5}$ ppm, $C_{BARE} = 200$ ppm, respectively). Thus, the calculated EF is 3.08×10^6.

Furthermore, the repeatability and uniformity of SERS substrates were also investigated as shown in Fig. 5c. Ten locations on SERS substrate were randomly selected for Raman measurement with 1 ppm RhB concentration. The uniformity of the SERS signal is estimated by the relative standard deviation (RSD) of the peak intensity of 1645 cm^{-1}. The RSD value is 3.29%, as shown in Fig. 5d.

In addition, to evaluate the reliability of SERS substrate based on Ag/ZnO porous membrane, fifteen chosen at random points on the substrate dropped with 1 ppm RhB were used in three distinct samples made under the same synthesis conditions for SERS measurement (Fig. 6a). The uniformity of the SERS signal is estimated by the relative standard deviation (RSD) of the peak intensity of 1645 cm^{-1} with the value of 9.36%, 6.56%, and 6.80%, respectively (Fig. 6b). The relatively low RSD values indicate that the substrates have good uniformity, and the SERS signal can be reproduced from different locations.

To verify the long-term stability of the Ag/ZnO porous membrane substrate, SERS spectra with 1 ppm RhB were detected after 30, 45, and 60 days as shown in Fig. 7. The unchanged SERS signals after 60 days testing indicate the Ag/ZnO porous membrane substrates having excellent oxidation resistance and being stored at room temperature for long periods. Furthermore, RhB is a prohibited food additive, and detecting it in practical samples is important. Here, to demonstrate the practical applicability, SI Fig. S2 shows a comparison of SERS sensing signals of our Ag/ZnO samples toward (i) 1 ppm of RhB in water and (ii) 1 ppm of RhB in Chilli powder solution. As found, their Raman spectra are similar regarding the positions of characteristic peaks of RhB, and that finally confirms the potential of our Ag/ZnO porous membrane in practical detection of RhB.

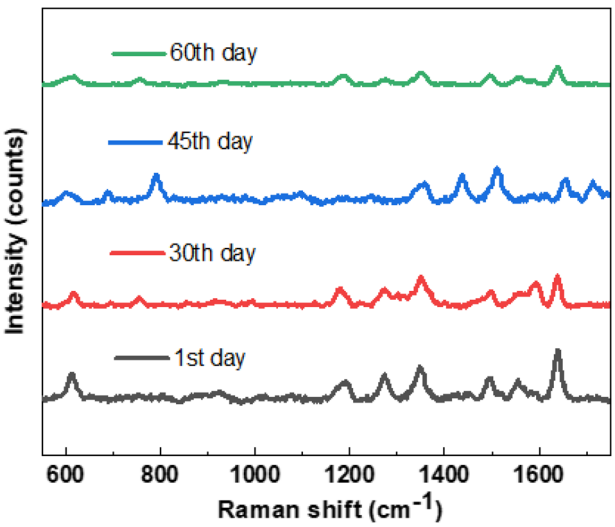

Fig. 7 The durability of SERS substrate under measuring over 60 days.

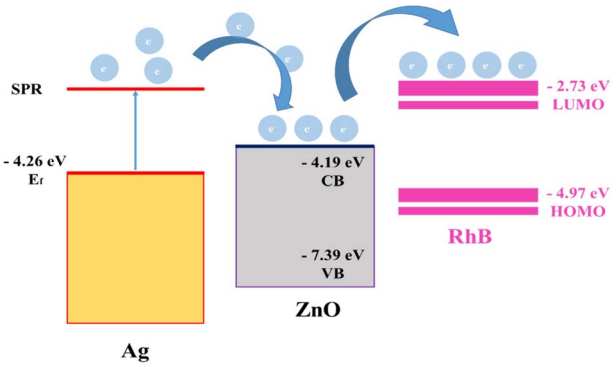

Fig. 8 Schematic of charge transfer mechanism between Ag, ZnO, and RhB.

3.3. SERS mechanisms of Ag/ZnO porous membrane

The high SERS enhancement of RhB on the Ag/ZnO porous membrane can be clarified by both EM and CM mechanisms. In which, the EM is explained through LSPR effect of Ag NPs, while CM is caused by ZnO NPs. Indeed, in EM mechanism, "hot spots" are created not only at interface between Ag NPs and ZnO, but also Ag NPs of neighboring insides of pores.[24] These "hot spots" enhance the Raman signal effectively. Besides, the CM mechanism also contributes to enhancing the SERS signal. Indeed, the conduction band and valence band of ZnO are at −4.19 eV and −7.39 eV, respectively (with a band gap of 3.2 eV), while the positions of RhB's highest occupied molecular orbital (HOMO) and lowest unoccupied molecular orbital (LUMO) are −4.97 eV and −2.73 eV.[37] According to Fig. 8, the conduction band of ZnO is between the Fermi energy level of Ag (−4.26 eV) and the LUMO of Rhodamine B (−2.73 eV). When the LSPR of Ag NPs happens, the hot electrons transfer from SPR level of Ag NPs to ZnO membrane until their Fermi energy levels reached equilibrium. This charge redistribution phenomenon leads to a change in the distribution within the negatively charged ZnO region, the positively charged Ag region, and the high charge density at the Ag/ZnO interface.[24] It enables a local electric field that can enhance the Raman scattering of RhB. Moreover, the highly porous structure further increased the absorption capacity and interaction time between the excitation photon and the target molecules, which contributed to explaining the enhanced Raman signal of the Ag/ZnO porous membrane sample.

4. Conclusion

Summary, Ag/ZnO porous membranes were successfully fabricated for SERS application to detect Rhodamine B at low concentration. Ag NPs were uniformly assembled on the side surfaces of ZnO porous membrane by the chemical silver reaction method. The working principle of SERS are clarified through both EM and CM mechanism. More interestingly, the high-density pores prolong the interaction between photon and target molecules. As a results, the Ag/ZnO porous membrane exhibited a high SERS sensitivity for RhB detection with the

limit of detection (LOD) and enhancement factor (EF) of 7.9 × 10^{-6} ppm and 3.08 × 10^{6}, respectively. However, for practical use, the selectivity of the Ag and ZnO combination toward RhB is of concern. Indeed, there are many reports using Ag and ZnO for detecting organic compounds. Regardless, this study showed the benefit of using the nanoporous membrane structure of Ag/ZnO to enhance the SERS sensing signal. With further surface functionalization or treatment (to tune the CM mechanism), we believe that nanoporous SERS substrates will be levelled up and more promising for more selectively detecting toxic organic compounds, contributing to the improvement of human quality of life.

Author contributions

T. N. T. Nguyen: conceptualization, writing – original draft; N. T. H. Nguyen: formal analysis M. K Tran: investigation; L. T. Duy: methodology; H. N. Luong: investigation; H. D. Tong: methodology; T. T. Pham: data curation; V. Q. Dang: supervision, writing – review & editing.

Conflicts of interest

There are no conflicts to declare.

Data availability

The authors confirm that the data supporting the findings of this study are available within the article and its supplementary information (SI). Supplementary information: additional SEM data and demonstration of practical RhB detection. See DOI: **https://doi.org/10.1039/d5ra06188a**.

Acknowledgements

This research is funded by Ho Chi Minh City University of Technology and Education under grant number: T2024 – 61.

References

1 X. Wang, E. Zhang, H. Shi, Y. Tao and X. Ren, Semiconductor-based surface enhanced Raman scattering (SERS): from active materials to performance improvement, *Analyst*, 2022, **147**, 1257–1272, DOI: **10.1039/D1AN02165F**.

2 S. M. Restaino and I. M. White, A critical review of flexible and porous SERS sensors for analytical chemistry at the point-of-sample, *Anal. Chim. Acta*, 2019, **1060**, 17–29, DOI: **10.1016/j.aca.2018.11.057**.

3 J. Zheng and L. He, Surface-Enhanced Raman Spectroscopy for the Chemical Analysis of Food, *Compr. Rev. Food Sci. Food Saf.*, 2014, **13**, 317–328, DOI: **10.1111/1541-4337.12062**.

4 W. Xie, P. Qiu and C. Mao, Bio-imaging, detection and analysis by using nanostructures as SERS substrates, *J. Mater. Chem.*, 2011, **21**, 5190–5202, DOI: **10.1039/C0JM03301D**.

5 J. Q. Li, P. V. Dukes, W. Lee, M. Sarkis and T. Vo-Dinh, Machine learning using convolutional neural networks for SERS analysis of biomarkers in medical diagnostics, *J. Raman Spectrosc.*, 2022, **53**, 2044–2057, DOI: **10.1002/jrs.6447**.

6 P. S. Priya, P. P. Nandhini, S. Vaishnavi, V. Pavithra, M. H. Almutairi, B. O. Almutairi, S. Arokiyaraj, R. Pachaiappan and J. Arockiaraj, Rhodamine B, an organic environmental pollutant induces reproductive toxicity in parental and teratogenicity in F1 generation in vivo, *Comp. Biochem. Physiol., Part C: Toxicol. Pharmacol.*, 2024, **280**, 109898, DOI: **10.1016/j.cbpc.2024.109898**.

7 M. Arabi, A. Ostovan, A. R. Bagheri, X. Guo, J. Li, J. Ma and L. Chen, Hydrophilic molecularly imprinted nanospheres for the extraction of Rhodamine B followed by HPLC analysis: A green approach and hazardous waste elimination, *Talanta*, 2020, **215**, 120933, DOI: **10.1016/j.talanta.2020.120933**.

8 J. Wu, W. Liu, R. Zhu and X. Zhu, On-line separation/analysis of Rhodamine B dye based on a solid-phase extraction high performance liquid chromatography self-designed device, *RSC Adv.*, 2021, **11**, 8255–8263, DOI: **10.1039/d0ra10771a**.

9 L. Yang, Y. Peng, Y. Yang, J. Liu, H. Huang, B. Yu, J. Zhao, Y. Lu, Z. Huang, Z. Li and J. R. Lombardi, A Novel Ultra-Sensitive Semiconductor SERS Substrate Boosted by the Coupled Resonance Effect, *Adv. Sci.*, 2019, **6**, 1900310, DOI: **10.1002/advs.201900310**.

10 R. Lu, J. Sha, W. Xia, Y. Fang, L. Gu and Y. Wang, A 3D-SERS substrate with high stability: Silicon nanowire arrays decorated by silver nanoparticles, *CrystEngComm*, 2013, **15**, 6207–6212, DOI: **10.1039/C3CE40788H**.

11 S. Yüksel, M. Ziegler, S. Goerke, U. Hübner, K. Pollok, F. Langenhorst, K. Weber, D. Cialla-May and J. Popp, Background-Free Bottom-Up Plasmonic Arrays with Increased Sensitivity, Specificity and Shelf Life for SERS Detection Schemes, *J. Phys. Chem. C*, 2015, **119**, 13791–13798, DOI: **10.1021/acs.jpcc.5b01389**.

12 J. Peng, Y. Song, Y. Lin and Z. Huang, Introduction and Development of Surface-Enhanced Raman Scattering (SERS) Substrates: A Review, *Nanomaterials*, 2024, **14**, 1648, DOI: **10.3390/nano14201648**.

13 C. Lee, C. S. Robertson, A. H. Nguyen, M. Kahraman and S. Wachsmann-Hogiu, Thickness of a metallic film, in addition to its roughness, plays a significant role in SERS activity, *Sci. Rep.*, 2015, **5**, 11644, DOI: **10.1038/srep11644**.

14 G. Macias, M. Alba, L. F. Marsal and A. Mihi, Surface roughness boosts the SERS performance of imprinted plasmonic architectures, *J. Mater. Chem. C*, 2016, **4**, 3970–3975, DOI: **10.1039/C5TC02779A**.

15 Y. Lu, X. Zhang, L. Zhao, H. Liu, M. Yan, X. Zhang, K. Mochizuki and S. Yang, Metal-organic framework template-guided electrochemical lithography on substrates for SERS sensing applications, *Nat. Commun.*, 2023, **14**, 5860, DOI: **10.1038/s41467-023-41563-5**.

16 L. Bi, X. Wang, X. Cao, L. Liu, C. Bai, Q. Zheng, J. Choo and L. Chen, SERS-active Au@Ag core-shell nanorod (Au@AgNR) tags for ultrasensitive bacteria detection and antibiotic-susceptibility testing, *Talanta*, 2020, **220**, 121397, DOI: **10.1016/j.talanta.2020.121397**.

17 V.-T. Vo, V.-D. Phung and S.-W. Lee, Nanosilver-embedded silicon nanowires as a SERS-active substrate for the ultrasensitive detection of monoamine neurotransmitters, *Surf. Interfaces*, 2021, **25**, 101181, DOI: 10.1016/j.surfin.2021.101181.

18 W. Zhang, B. Li, L. Chen, Y. Wang, D. Gao, X. Ma and A. Wu, Brushing, a simple way to fabricate SERS active paper substrates, *Anal. Methods*, 2014, **6**, 2066–2071, DOI: 10.1039/C4AY00046C.

19 X. Qiu, J. Gu, T. Yang, C. Ma, L. Li, Y. Wu, C. Zhu, H. Gao, Z. Yang, Z. Wang, X. Li, A. Hu, J. Xu, L. Zhong, J. Shen, A. Huang and G. Chen, Sensitive determination of Norfloxacin in milk based on β-cyclodextrin functionalized silver nanoparticles SERS substrate, *Spectrochim. Acta, Part A*, 2022, **276**, 121212, DOI: 10.1016/j.saa.2022.121212.

20 L. Yang, Y. Yang, Y. Ma, S. Li, Y. Wei, Z. Huang and N. V. Long, Fabrication of Semiconductor ZnO Nanostructures for Versatile SERS Application, *Nanomaterials*, 2017, **7**, 398, DOI: 10.3390/nano7110398.

21 L. He, C. Liu, J. Hu, W. Gu, Y. Zhang, L. Dong, X. Fu and J. Tang, Hydrophobic ligand-mediated hierarchical Cu nanoparticles on reduced graphene oxides for SERS platform, *CrystEngComm*, 2016, **18**, 7764–7771, DOI: 10.1039/C6CE01728B.

22 S. Cui, Z. Dai, Q. Tian, J. Liu, X. Xiao, C. Jiang, W. Wu and V. A. L. Roy, Wetting properties and SERS applications of ZnO/Ag nanowire arrays patterned by a screen printing method, *J. Mater. Chem. C*, 2016, **4**, 6371–6379, DOI: 10.1039/C6TC00714G.

23 T. Dong, Y. Wu and M. Mei, Hierarchically porous coralloid ZnO@Ag microspheres as SERS substrate for highly sensitive malachite green detection, *Opt. Mater.*, 2024, **152**, 115405, DOI: 10.1016/j.optmat.2024.115405.

24 H. N. Luong, N. M. Nguyen, L. N. T. Nguyen, C. K. Tran, T. T. Nguyen, L. T. Duy, N. P. Nguyen, T. M. H. Huynh, T. T. Tran, B. T. Phan, T. V. T. Thi and V. Q. Dang, Detection of carbendazim by utilizing multi-shaped Ag NPs decorated ZnO NRs on patterned stretchable substrate through surface-enhanced Raman scattering effect, *Sens. Actuators, A*, 2022, **346**, 113816, DOI: 10.1016/j.sna.2022.113816.

25 T. M. Dinh, H. Q. Huynh, T. M. N. Mai, H. S. Truong, H. N. Luong, N. P. Nguyen, C. K. Tran, B. T. Phan and V. Q. Dang, Enhancing the performance of photodetectors based on ZnO nanorods decorated with Ag nanoparticles, *Semicond. Sci. Technol.*, 2021, **36**, 045009, DOI: 10.1088/1361-6641/abe21a.

26 G. Wisz, I. Virt, P. Sagan, P. Potera and R. Yavorskyi, Structural, Optical and Electrical Properties of Zinc Oxide Layers Produced by Pulsed Laser Deposition Method, *Nanoscale Res. Lett.*, 2017, **12**, 253, DOI: 10.1186/s11671-017-2033-9.

27 S. Lin, W.-L.-J. Hasi, X. Lin, S. Han, X.-T. Lou, F. Yang, D.-Y. Lin and Z.-W. Lu, Rapid and sensitive SERS method for determination of Rhodamine B in chili powder with paper-based substrates, *Anal. Methods*, 2015, **7**, 5289–5294, DOI: 10.1039/C5AY00028A.

28 J. Zhang, X. Li, X. Sun and Y. Li, Surface Enhanced Raman Scattering Effects of Silver Colloids with Different Shapes, *J. Phys. Chem. B*, 2005, **109**, 12544–12548, DOI: 10.1021/jp050471d.

29 N. T. Huyen, L. T. Q. Xuan, T. A. S. Suong, C. T. Thanh, P. V. Trinh, N. V. Tu, N. T. Loan, L. T. Q. Ngan, P. T. Binh, C. T. L. Huong, D. N. Thuan, V. X. Hoa, N. V. Hao, N. V. Quynh, H. Abe and N. V. Chuc, A novel approach for the fabrication of SERS substrates based on 3D urchin-like TiO2@Gr–AuNPs architecture, *RSC Adv.*, 2025, **15**, 15806–15818, DOI: 10.1039/D5RA02160J.

30 Y. Chen, W. H. Tse, L. Chen and J. Zhang, Ag nanoparticles-decorated ZnO nanorod array on a mechanical flexible substrate with enhanced optical and antimicrobial properties, *Nanoscale Res. Lett.*, 2015, **10**, 106, DOI: 10.1186/s11671-014-0712-3.

31 J. Chen and X. Zhu, Magnetic solid phase extraction using ionic liquid-coated core–shell magnetic nanoparticles followed by high-performance liquid chromatography for determination of Rhodamine B in food samples, *Food Chem.*, 2016, **200**, 10–15, DOI: 10.1016/j.foodchem.2016.01.002.

32 A. A. Ahmed Bakheet and X. shi Zhu, Determination of Rhodamine B in Food Samples by Fe3O4@ Ionic Liquids-β-Cyclodextrin Cross Linked Polymer Solid Phase Extraction Coupled with Fluorescence Spectrophotometry, *J. Fluoresc.*, 2017, **27**, 1087–1094, DOI: 10.1007/s10895-017-2042-1.

33 Z. Erbas and M. Soylak, Determination of Rhodamine B by UV–Vis spectrophotometry in cosmetics after microextraction by using heat-induced homogeneous liquid–liquid extraction method, *J. Iran. Chem. Soc.*, 2022, **19**, 3935–3942, DOI: 10.1007/s13738-022-02579-8.

34 W. Wei, Z. Xi and Q. Huang, Fabrication of SERS-active Au@Au@Ag double shell nanoparticles for low-abundance pigment detection, *Chin. J. Chem. Phys.*, 2021, **34**, 197–202, DOI: 10.1063/1674-0068/cjcp2005062.

35 T. T. H. Pham, X. H. Vu, N. D. Dien, T. T. Trang, T. T. K. Chi, P. H. Phuong and N. T. Nghia, Ag nanoparticles on ZnO nanoplates as a hybrid SERS-active substrate for trace detection of methylene blue, *RSC Adv.*, 2022, **12**, 7850–7863, DOI: 10.1039/D2RA00620K.

36 N. H. T. Tran, T. T. T. Van, H. Van Le, H. K. T. Ta and D. Van Hoang, Study of Ag NPs decorated - ZnO nanoflowers for the SERS - Based detection of pesticides: An experimental approach, *Mater. Chem. Phys.*, 2025, **337**, 130612, DOI: 10.1016/j.matchemphys.2025.130612.

37 X. Chen, L. Zhu, Z. Ma, M. Wang, R. Zhao, Y. Zou and Y. Fan, Ag Nanoparticles Decorated ZnO Nanorods as Multifunctional SERS Substrates for Ultrasensitive Detection and Catalytic Degradation of Rhodamine B, *Nanomaterials*, 2022, **12**, 2394, DOI: 10.3390/nano12142394.